Influence of temperature on the atmospheric corrosion of the MgAl alloy AM50 produced by semi-solid cast and high pressure die cast techniques

Mohsen Esmaily[a], Mehrdad Shahabi-Navid[a], Jan-Erik Svensson[a], Mats Halvarsson[b], Lars Nyborg[c], Yu Cao[c], Lars-Gunnar Johansson[a]

a Department of Chemical and Biological Engineering, Chalmers University of Technology, SE-412 96 Göteborg, Sweden
b Department of Applied Physics, Chalmers University of Technology, SE-412 96 Göteborg, Sweden
c Department of Materials & Manufacturing Technology, Chalmers University of Technology, 2A, SE-412 96 Göteborg, Sweden

Abstract

The effect of temperature on the atmospheric corrosion of the MgAl alloy AM50 was investigated in the laboratory. The alloy was investigated in both semi-solid cast and high pressure die cast form. Polished samples were exposed to air containing 400ppm CO_2 for up to 4 weeks at 22ºC, 4ºC and -4ºC at 95% relative humidity (RH). The rate of corrosion was determined by mass gain and metal loss measurements. The corrosion products were analyzed by SEM/EDX. Analysis by XRD showed that the composition of the crystalline corrosion product depended on the exposure temperature. Both materials exhibited a strong positive correlation between temperature and the rate of NaCl-induced atmospheric corrosion. It is suggested that the temperature dependence of corrosion is related to the dissolution of alumina in the passive film. The semi-solid cast material exhibited lower average corrosion rates at all three temperatures.

Keywords: *NaCl-induced atmospheric corrosion, magnesium alloy, temperature effect, corrosion products.*

* Corresponding author at: Department of Chemical and Biological Engineering, Chalmers University of Technology, SE-412 96 Göteborg, Sweden

Email address: mohsen.esmaily@chalmers.se
Phone: 0046-317722864

1. Introduction

Magnesium-aluminum (MgAl) alloys combine high specific strength with good castability. The alloys are widely used in the automotive industry. However, the relatively low corrosion resistance limits their application [1,2]. Components made from MgAl alloys are commonly produced by high-pressure die casting (HPDC). The oxides formed during the turbulent filling function as local stress concentrators and can degrade the mechanical properties of the castings [3,4]. Alternatively, semi-solid casting technology can be used to produce complex components. Previous studies reported on a number of advantages of semi-solid cast Mg alloys over their liquid cast counterparts [5,6]. The present study includes material produced by Rheocasting (RC) where a semi-solid slurry is used, which shows non-turbulent or thixotropic flow behavior.

Because MgAl alloys are often exposed to atmospheric conditions at ambient temperatures, a better understanding of the atmospheric corrosion properties is of industrial importance. One of the most important corrosion accelerators in the atmosphere is NaCl which is used for deicing of roads in the wintertime. Hence, the atmospheric corrosion behaviour of MgAl alloys at low temperature is of interest. In a preliminary study, the authors investigated the influence of temperature on the NaCl-induced atmospheric corrosion behavior of HPDC AM50 in the presence and absence of CO_2 [7]. The results showed a strong positive temperature dependence for corrosion. Chen et al. [8] has reported on a positive correlation between corrosion attack and temperature for the initial stages (2h) of atmospheric corrosion of the MgAl alloy AZ91 between 2^oC and 8^oC. Information on NaCl-induced atmospheric corrosion behavior of semi-solid cast MgAl alloys and how it compares to the same alloy in the HPDC state is practically absent in the literature. Also, the atmospheric corrosion behavior of semi-solid MgAl alloy at minus temperatures is not known. Thus, the present paper investigates the atmospheric corrosion behavior of alloy AM50 at different temperatures for two casting methods: RC and HPDC.

2. Experimental procedures

2.1. Sample preparation

HPDC and RC AM50 alloy with a nominal composition of 5%Al, 0.01%Zn, 0.25%Mn, balance Mg (by weight), was employed in this investigation. 99.97% Mg was used as a reference material. Corrosion coupons were machined with approximate size of 2×15×15 mm^3 and a geometrical area of about 5.5 cm^2. Care was taken to avoid the outermost part of

the cast as well as the central regions. The samples were ground by SiC papers from P1000 to P4000 mesh. Polishing was done using cloth discs and diamond paste in the range of 1-3 µm, followed by a fine polishing step via OPS colloidal silica for 120s. The samples were contaminated with two different amounts of salt, 14 and 70 µg/cm^2. Duplicate and triplicate samples were used for each condition to increase reliability of the data.

2.2. Atmospheric corrosion exposures

The experimental set-up for the exposures at ambient and below ambient temperatures has been described in [7]. The gas flow used is 1000 mL/min corresponding to an average flow velocity of 1mm/s. Relative humidity (RH) is regulated to be 95+-0.3%. CO_2 is added from a cylinder to give a constant concentration of 400±20ppm. To perform corrosion experiments at sub-zero temperature, a new corrosion system was designed and developed. Ethylene glycol was used as antifreeze.

2.3. Analytical techniques

The mass gain was recorded using a six decimal balance. The metal loss was determined by leaching and pickling the corroded specimens in 20%CrO_3(aq) using ultrasonic agitation. The pickling procedure is described elsewhere [7]. The gravimetric data was used to calculate the ratio between total corrosion product mass and metal loss. Crystalline corrosion products formed under various exposure conditions were analyzed by X-ray diffraction (XRD) using a Bruker AXS D8 powder diffractometer. The system was equipped with grazing incidence beam attachment and a Göbel mirror. CrKα radiation (λ = 2.29 Å) was used and the angle of incidence was 5^o. The distribution of elements after exposure and pitting were studied using cross sections prepared by focused ion beam milling (FIB) using a FEI Dual Beam system. The FIB method was used because a precise positioning of the cross section was required. The electron column is equipped with a FEG and the ion column had a liquid gallium source. The morphology of the corrosion products was examined by an FEI Quanta 200 environmental scanning electron microscopy (ESEM). The instrument was equipped with Oxford Inca energy dispersive X-ray detector (EDX) system. SEM/EDX was used for local chemical analysis and for elemental mapping of the milled cross sections. A ToF-SIMS V spectrometer was used to analyze the corroded surfaces after corrosion exposures. A pulsed 20 keV Bi^+ primary ion source was employed. The total primary ion flux was below 10^{12}ions/cm ^{2} to ensure static conditions. A lateral resolution of 200–300 nm and a sampling depth of ~10-20 Å was achieved with this setting.

3. Results

Figure 1 shows typical as-cast microstructures of RC and HPDC AM50. The as-cast microstructure of alloy AM50 consists of primary α-Mg dendrites and secondary α-Mg dendrites (also termed inter-dendritic regions) [1]. The latter regions are decorated by intermetallic, high Al phases, *i.e.*, β ($Mg_{17}Al_{12}$) and η (Al_8Mn_5) particles. The EDX results indicated that the average Al content of the β phase was 34% (by weight) while the η phase was composed of 30% Al, 33% Mn, 0.6%Fe, the balance being Mg. In the RC microstructure the α-Mg grains tend to be globular while they have a more dendritic structure in the HPDC alloy (Fig. 1a and b). The investigation also showed that the β phase tends to be more continuous in the RC material compared to the HPDC alloy.

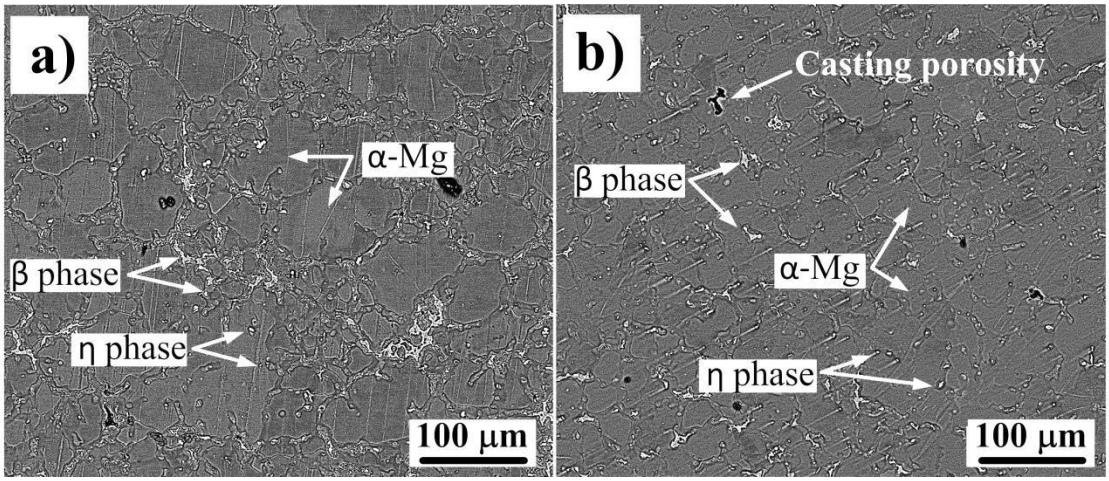

Fig. 1. Microstructures of the investigated magnesium alloys, (a) RC AM50 alloy and (b) HPDC AM50 alloy.

Table 1 shows the crystalline corrosion products identified after 672h exposure at -4, 4 and 22ºC. The ratio between total mass and metal mass of the corrosion products is also provided (compare Table 2). In the absence of salt, no crystalline corrosion product was detected. In the presence of NaCl three different magnesium hydroxy carbonates were identified namely giorgiosite, hydromagnesite and $Mg_5(CO_3)_4(OH)_2{\times}5H_2O$. In some cases the diffractograms contained additional weak diffraction peaks (U2 in Table 1) that could not be attributed to a known compound. The crystalline phases detected at 4 and 22ºC were identical.

Table. 1. Crystalline phases identified by XRD at all the three temperatures.

Name	***Formula***	***abbreviation***	***Corrosion product ratio****
Hydromagnesite	$Mg_5(CO_3)_4(OH)_2x4H_2O$	H4	3.85
	$Mg_5(CO_3)_4(OH)_2x5H_2O$	H5	4.00
Giorgiosite	$Mg_5(CO_3)_4(OH)_2x8H_2O$	H8	4.44

Exposure conditions	***-4°C***	***4 and 22°C***
No NaCl – 400ppm CO_2	U1	No corrosion products
NaCl - 400ppm CO_2	U1	H8, H5, H4, U2

***** Total mass / mass of metal ions

In contrast, no crystalline corrosion products could be identified after corrosion in the presence of NaCl at -4°C. Instead an unknown crystalline phase (U1 in Table 1) appeared on all samples. The gravimetric results at -4, 4 and 22ºC with different amounts of NaCl are presented in Table 2. The ratio between the mass of the corrosion products and the metal loss is also provided for each case. This value reflects the average corrosion product composition and can be compared to the corresponding ratios of selected corrosion products in Table 1. The measured corrosion product ratios agree well with the three magnesium hydroxy carbonates identified by XRD.

As expected, corrosion is very slow in the absence of NaCl (reference runs). Also, the extent of corrosion is correlated with the amount of salt added. Decreasing the temperature from 22°C to -4°C resulted in a considerable decrease of the average corrosion rates, irrespective of the amount of salt. Thus, the rate of corrosion of RC and HPDC AM50 at -4°C is lower by a factor of 11 and 12 respectively, compared to 22°C. In contrast, there is no clear correlation between temperature and corrosion rate for 99.97%Mg, the average dry mass gain being 6.8, 9.3, 5.1 mg/cm^2 at -4, 4 and 22ºC, respectively.

Table 2. Average dry mass gains, metal loss, corrosion product ratio and corrosion rates for HPDC and RC AM50.

Temp. (°C)	NaCl (μg/cm^2)	Average dry mass gain (mg/cm^2)		Metal loss (□g/cm^2)		Ratio		Corrosion rate (μm/year)	
		RC	HPDC	RC	HPDC	RC	HPDC	RC	HPDC
	Ref.	0.06	0.04	0.03	0.02	3.7	4.0*	1	1
22	14	0.60	0.74	0.21	0.26	3.9	3.8	15	19
	70	1.59	2.41	0.57	0.96	3.8	3.5	42	70
	Ref.	0.03	0.01	0.01*	0.01	4.0*	4.0*	-	-
4	14	0.12	0.18	0.05	0.05	3.4	3.7	4	3
	70	0.50	1.31	0.16	0.64	4.7	3.5	12	47
	Ref.	0.01	0.01	<0.01	0.01	4.0*	4.5	<1	<1
-4	14	0.07	0.08	0.03	0.04	3.0	3.1	2	3
	70	0.15	0.20	0.06	0.09	3.6	3.2	4	6

The results show that the RC material consistently exhibits lower average corrosion rates compared to the HPDC material. The effect is especially noticeable at 4°C with 70 μg/cm^2 NaCl where the average mass gain is 2.6 times higher for the HPDC material. Figure 2 illustrates the effect of exposure temperature on the corrosion morphology. In accordance with the gravimetric results, the corrosion attack is most severe for the samples with the largest amount of added salt (70 μg/cm^2). Also an increase in temperature from -4ºC to 22ºC significantly increases the amount of corrosion products on both alloys. The general morphology of corrosion products is relatively uniform with conspicuous circular features that reflect the location of the NaCl(aq) electrolyte droplets formed upon starting the corrosion

exposure. The surface coverage of NaCl crystallites after the exposures is shown in Fig. 2. The NaCl crystallites correspond to the recrystallization of NaCl(aq) electrolyte that was present when the corrosion exposure ended. It may be noted that while NaCl was present throughout the exposures, providing an electrolyte, the amount of salt decreased with exposure time. The consumption of salt is due to the formation of corrosion products containing sodium and chlorine. Thus, sodium becomes associated with carbonate and chlorine with magnesium as a result of corrosion. The surface coverage of NaCl(s) after exposure was less for the HPDC material at all three temperatures, indicating that more salt is consumed in that case.

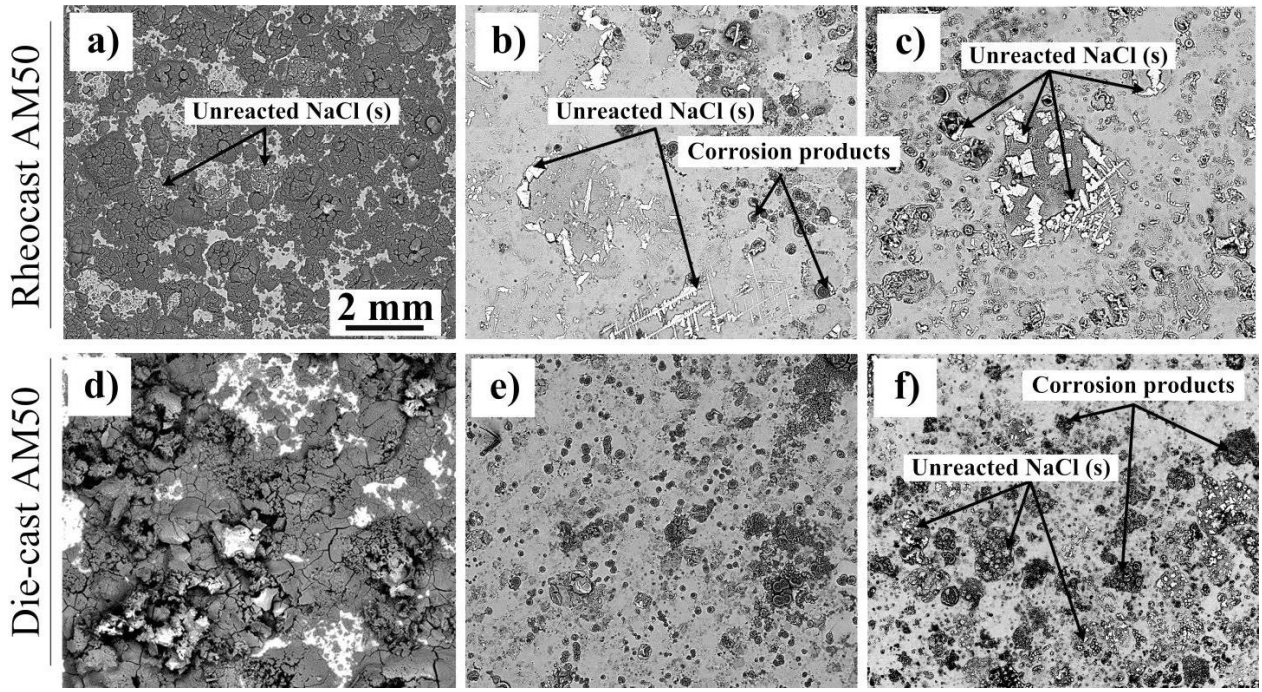

Fig. 2. The effect of temperature on corrosion morphology on the samples with 70µgcm^{-2} NaCl in the presence of 400ppm CO_2; (a) RC AM50 at 22ºC, (b) RC AM50 at 4ºC, (c) RC AM50 at -4ºC (d) HPDC AM50 at 22ºC, (e) HPDC AM50 at 4ºC (f) HPDC AM50 at -4ºC.

Figure 3 illustrates the redistribution of Na^+ and Cl^- ions on the corroded alloy AM50. Thus, the *ToF*-SIMS results indicate that Na^+ ions are enriched on the uncorroded metal surface. The EDX analysis of the cross sections demonstrated that chloride tends to accumulate in the pits and at the alloy/corrosion product interface.

4. Discussion

Under the experimental conditions, the NaCl added before exposure forms an aqueous solution on the metal surface. MgAl alloys immersed in NaCl(aq) solution are known to corrode by an electrochemical process, where the anodic dissolution of magnesium and the

cathodic reduction of water occurs at different sites [9, 10]. In the present study, the electrochemical nature of corrosion is demostrated by the redistribution of sodium and chloride ions after the corrosion exposure, see Fig. 3. Thus, the chloride ions accumulated in the corrosion pits while the sodium ions were observed to accumulate at a distance from the location of the corrosion attack, indicating the presence of cathodic sites. The results show that the atmospheric corrosion of both RC and HPDC materials exhibits a strong positive temperature dependence (see Table 2 and Fig. 2). Thus, at -4^{o}C the corrosion of alloy AM50 is about 11-12 times slower than that at 22^{o}C. In contrast, the atmospheric corrosion of 99.97%Mg did not show a clear temperature dependence. It has been reported that the NaCl-induced atmospheric corrosion of Al shows similar strong positive temperature dependence [11]. This hints that the slowing of the rate of corrosion of alloy AM50 at 4 and -4^{o}C is related to the Al content in the alloy.

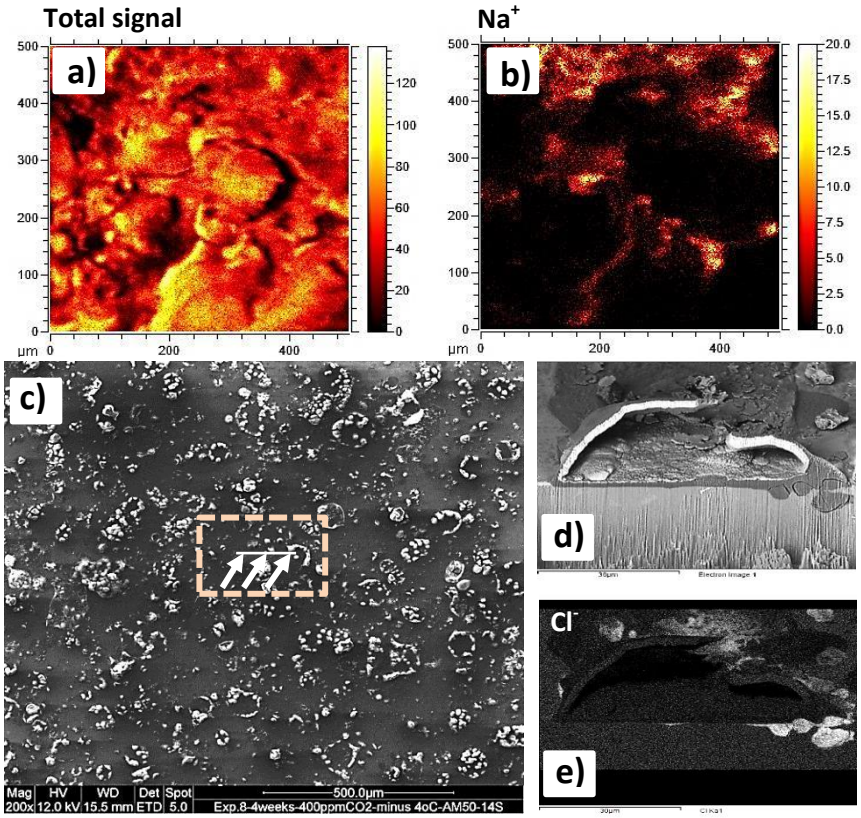

Fig. 3. (a) ToF-SIMS (all cations) image of HPDC alloy AM50 after 672h exposure with 400ppm CO_2 and 70 µg/cm^2 NaCl at 22°C, (b) the corresponding ToF-SIMS Na^+ map, (c) top-view SEM-BSE micrograph of HPDC AM50 after 672h exposure with 400ppm CO_2 and 14 µg/cm^2 NaCl at -4°C, (d) and (e) the corresponding FIB-prepared cross section as indicated in (c) and the chlorine EDX map.

It is suggested that the temperature dependence of corrosion is related to the dissolution of alumina in the passive film. The corrosion product composition is also strongly affected by exposure temperature. The XRD diffraction patterns acquired from both RC and HPDC AM50 showed formation of a hitherto unknown crystalline corrosion product (U1) at -4ºC.

The results reveal that the average corrosion rate of the RC material is consistently lower than that of the HPDC material at all three temperatures. As the global chemical compositions are identical, the different corrosion behavior should be related to differences in microstructure. The preliminary qualitative results indicate that the fraction of β phase is higher in the RC material than in the HPDC material. It has been reported that a high fraction of β phase can improve the corrosion behavior of MgAl alloys by forming a physical barrier [12]. However, attributing the observed differences in atmospheric corrosion behavior to this effect would be premature. Thus, more studies are required to understand and correlate the influence of different microstructural configurations (as observed in RC and HPDC material) on the corrosion mechanism of the alloy AM50.

5. Conclusions

The atmospheric corrosion of alloy AM50 produced by semi solid and HPDC methods exhibited a strong positive correlation with the exposure temperature. It is suggested that the temperature dependence of NaCl-induced atmospheric corrosion of alloy AM50 is related to the dissolution of alumina in the passive film. The NaCl-induced atmospheric corrosion attack was in the order 99.97%Mg > HPDC AM50 > RC AM50. The better corrosion resistance of RC AM50 is attributed to the differences in the microstructure of the alloy produced by two casting technologies.

References

[1] Mordike, B. L., Ebert T., Materials Science and Engineering A **2001**, 37-45.
[2] Shi, Z., Song, G., Atrens, A., Corrosion Science **2005**, 2760-2777.
[3] Klein, F., in *Proceeding DGM Informationsgesellschaftsverlag*, Germany, **1992**, 53-60.
[4] Emley, E. F., Principals of Magnesium Technology, Pergamon Press, Oxford, **1966**, p. 142.
[5] Aguilar, J., Grimming, T., Bhrig-Polaczek, A., in Proceeding of the 6th International Conference Magnesium Alloy and Their Application, Wiley-VCH, Verlay GmbH&Co., **2003**, 767-773.
[6] Czerwinski, F., Zielinska-lipied, Z., Pinet, P. L., Overbeeke, J., Acta Materialia **2001**, 1225-1235.
[7] Esmaily, M., Shahabi-Navid, M., Svensson J-. E., Halvarsson, M., Nyborg, L., Cao, Y., Johansson, L-. G, *In press*.
[8] Chen, J., Wang, J. Q., Han, E. H., Ke, W., Corrosion Engineering **2011**, 277-284.
[9] Godard, H. P., Jepson, W., Bothwell, M., Lane, R. L., the Corrosion of Light Metals, Wiley and Sons, New York, **1967**.
[10] Song, G., Atrens, A., Advance Engineering Materials **1999**, 11-33.
[11] Blücher, D. B., Svensson, J-. E., Johansson L-. G., Rohwerder, M., Stratmann, M., Journal of Electrochemical Society **2004**, 621-626.
[12] Makar, G.L., Kruger, J., Sieradzki, K., Journal of Electrochemical Society **1992**, 47-53.